actuators

MDPI

Article

Structure Design and Optimization of the Radial Magnetic Bearing

Qiang Li [1], Yefa Hu [1,2] and Huachun Wu [1,2,*]

[1] School of Mechanical & Electronic Engineering, Wuhan University of Technology, Wuhan 430070, China
[2] Hubei Provincial Engineering Technology Research Center for Magnetic Suspension, Wuhan 430070, China
* Correspondence: whcwhut@whut.edu.cn

Abstract: According to different working environments and functional requirements, radial magnetic bearings (RMBs) have various design methods. Some methods' lack of effectiveness or accuracy is likely to cause significant differences in the structural performance of magnetic bearings, which will cause serious problems such as limited bearing capacity and complex control. This paper analyzes the structure topology of a magnetic bearing according to the application scenario of RMBs, then proposes a general design example of an 8-pole magnetic bearing based on magnetic circuit analysis and reveals the linearity between electromagnetic force and current as well as air gap through finite element analysis and the influence of magnetic saturation on the load capacity of the magnetic bearing structure. After completing the preliminary design, we further optimize the structure, take the genetic algorithm as an example to iterate the influence coefficient, and summarize and prospect. The design scheme and optimization method proposed in this paper only provide a valuable reference for researchers and factories when devising RMB devices.

Keywords: radial magnetic bearing; structure topology; finite element analysis; design scheme

Citation: Li, Q.; Hu, Y.; Wu, H. Structure Design and Optimization of the Radial Magnetic Bearing. *Actuators* **2023**, *12*, 27. https://doi.org/10.3390/act12010027

Academic Editor: Takeshi Mizuno

Received: 2 December 2022
Revised: 28 December 2022
Accepted: 4 January 2023
Published: 6 January 2023

1. Introduction

Radial magnetic bearings (RMBs) are new high-performance support devices with no friction between the rotor and the bearing. They offer more advantages than rolling bearings, such as high attainable rotating speeds, no lubrication, low losses, and tunable bearing dynamic parameters. Magnetic bearings are grouped into three primary structural configurations based on their working principles: active magnetic bearings (AMBs), passive magnetic bearings (PMBs), and hybrid magnetic bearings (HMBs). The AMB group is divided into direct-current (DC) and alternating-current (AC) magnetic bearing groups according to the bearings' starting current formation modes and cylindrical and conical magnetic bearing groups according to the stator and shape. Moreover, RMBs with DC control are widely used in AMBs [1].

Magnetic bearings are electromechanical hybrid systems, which include the rotor, stator, and electromagnet of the mechanical part, as well as the shaft position sensor, controller, and power amplifier (PA) of the control part [2]. Figure 1 shows the working principle of differential control of a single degree of freedom in RMBs. The stability of the suspension system is achieved by differential control, in which the output change voltage signal is detected by a non-contact proximity sensor due to the offset of the rotor shaft. Then an electromagnetic force counteracts the unbalanced force to attract the rotor back to its equilibrium position. The electromagnetic force is generated by differential currents in the two opposite coils output by the controller and the power amplifier [3]. This process happens instantaneously, thus levitating the rotor during the operation.

Magnetic bearings are now widely used in aerospace, transportation, and new energy fields, among others. AMBs are essential components of high-speed systems. The initial research and development investigated the magnetic bearing system with four-pole stator

topology [4,5]. The current of four coils in 4-pole RMBs is controlled by four independent PA or two symmetrical PA to generate electromagnetic forces in two vertical directions. At least three coils are necessary for a complete RMB to generate forces in two perpendicular directions. In recent years, the simplified three-pole structure has been frequently used in the field of miniature magnetic bearings to reduce power consumption and cost [6]. The 3-pole magnetic bearings can be driven in three ways, among which researchers have favored a three-phase converter drive in the past ten years because of its low cost and complexity [7,8]. However, the research on 3-pole RMBs focuses on the decoupling strategy and precise control of cross-coupling between magnetic poles due to its asymmetric structure. Some researchers use an increased number of magnetic poles to optimize the structure of a 3-pole magnetic bearing and finally form a unique 6-pole magnetic bearing [9]. Six-pole RMBs can be composed of three permanent magnet poles, three active poles, or six independent, active poles. In addition, the control benefit of using a three-phase converter drive is higher [10–12].

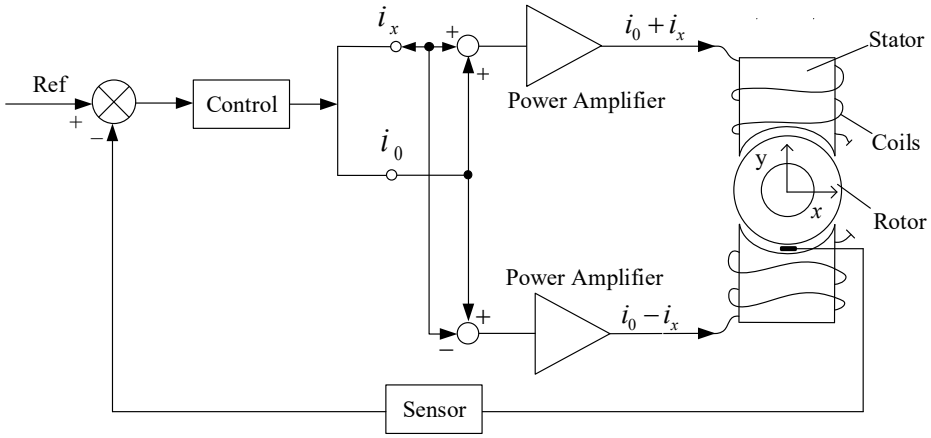

Figure 1. Working principle of an RMB system.

To improve the performance of 4-pole RMBs, researchers optimized them to form 8-pole RMBs, of which the most commonly used are heteropolar 8-pole RMBs [13,14]. Whether the cross-section of stator magnetic poles has the same magnetic polarity determines whether the structure is homopolar or heteropolar. Their diversity leads to different control methods and hysteresis losses. Generally, the stator and rotor are manufactured by laminating silicon steel sheets to reduce the change of magnetic field and eddy current loss. However, the heteropolar magnetic bearing suffers a more significant loss due to high-frequency magnetic field conversion during rotor rotation [15]. The C-type magnetic pole structure in heteropolar 8-pole RMBs is often formed by the distribution of magnetic poles as North-North-South-South (NNSS). The space between magnetic poles and electromagnetic force in the traditional C-type structure is not fully utilized, so some researchers propose to optimize it to form 12-pole E-type RMBs [16,17]. E-type magnetic pole structure divides one C-type magnetic pole into two small magnetic poles and places them on both sides of the other magnetic pole. The distribution of an e-type magnetic pole group in the form of SNS or NSN can ensure the independence of the magnetic circuit and reduce the probability of cross-coupling between magnetic poles [18,19]. Some 16-pole or 32-pole RMBs have better application effects on special occasions after combination or optimization [20–22].

Given the above design points of magnetic bearing, this paper has carried out a detailed analysis, proposed the design method of the structure ontology of RMBs, given an optimization scheme for the structure, and looked forward to the future research direction.

2. RMB Structure Topology

The function of the bearing is to support the rotating body of the machine, reduce the friction coefficient during its movement, and ensure its rotation accuracy. Magnetic bearings rely on electromagnetic force to overcome the rotor gravity and ensure the rotor rotation accuracy through the control system. The ontology structure of active RMBs mainly includes stators and rotors. We selected the appropriate topology for the required electromagnetic force according to the different application scenarios.

The stator structure of RMBs is similar to that of the motor stator, which is often formed by the lamination of soft magnetic materials. The stator structure is formed by bonding the thin, soft magnetic material, designing the winding coil according to the magnetic circuit, and then combining it with the conventional protective bearing. A complete rotor structure comprises a primary shaft and a shaft sleeve that realizes a particular function. Laminations of soft magnetic materials form the shaft sleeve at the matching position of the stator and rotor, and there is a unique measuring ring shaft sleeve at the measuring position of the sensor. Figure 2 shows a complete 4-DOF RMB device platform. The experimental platform uses the motor shaft to connect one end of the rotor as the transmission mode, and the coupling connection at the rotor port limits the axial offset of the rotor. The disc on the rotor is used to simulate the unbalanced force of the shaft, and other platform design methods can achieve different functional requirements.

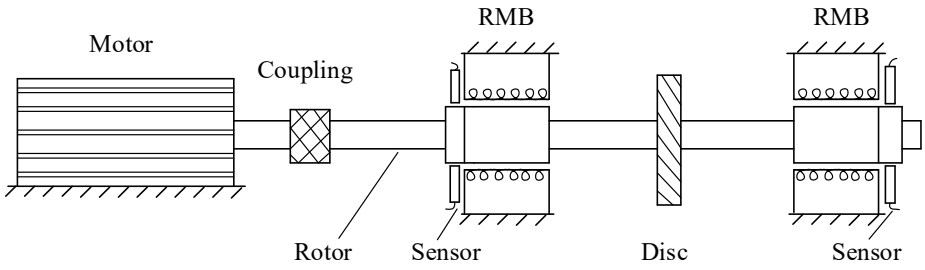

Figure 2. RMB device platform.

2.1. Four-Pole RMBs

Figure 3a shows the conventional 4-pole homopolar RMB structure, in which each pair of magnetic poles are distributed along the axial direction. There are only N poles or S poles along the circumferential direction. Figure 3b shows the 4-pole heteropolar RMB structure, and its magnetic polarity is arranged as NSNS. The direction parallel to the rotor gravity is called the y direction in this article, and the direction perpendicular to the gravity is called the x direction. In Figure 3b, the resultant force of electromagnetic force generated by currents i_1 and i_2 counteracts the rotor gravity in the y direction.

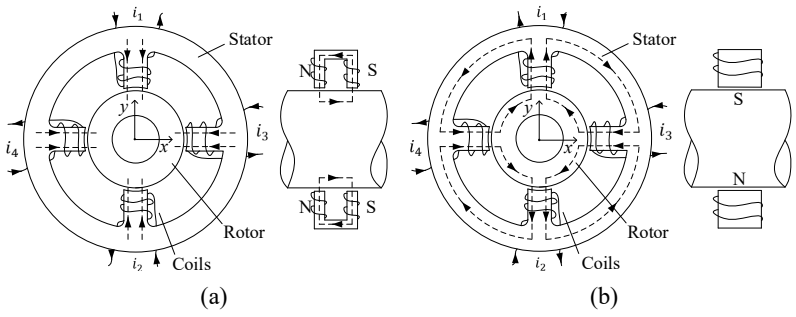

Figure 3. The 4-pole RMB structure. (**a**) Homopolar structure. (**b**) Heteropolar structure.

In contrast, the electromagnetic force generated by i_3 and i_4 keeps the rotating shaft rotating stably around the geometric axis. For homopolar RMBs, the magnetic field change around the rotor is small, and the eddy current generated is negligible. The superposition

of soft magnetic materials is usually used to reduce the hysteresis and eddy current loss in the stator structure of heteropolar RMBs.

The loss of magnetic bearing mainly includes power amplifier loss, copper loss, and iron loss (hysteresis loss and eddy current loss). Its loss has been low compared with traditional bearings, but power consumption is the leading performance standard for large heavy-duty, high-power equipment, and other special applications. For example, flywheel energy storage is mainly to reduce loss. Many articles have studied how to reduce the loss of magnetic bearings, mainly in three aspects. The first approach combines permanent magnets and electromagnets to form a new hybrid magnetic bearing [23]. The second approach is to improve the magnetic pole structure, such as reducing the number of magnetic poles to form a more straightforward magnetic pole structure or adopting a homopolar structure to reduce magnetic loss [24]. The third approach is to adopt a zero-bias current control method. Among them, the most widely used approach is to adopt a permanent magnet combination and improve the magnetic pole structure. For the 4-pole RMBs, researchers further simplified the magnetic pole structure and developed new 3-pole RMBs to reduce the loss.

2.2. Three-Pole RMBs and Six-Pole RMBs

Three-pole RMBs apply fewer power amplifiers, have lower re-magnetization frequencies (thus reducing the iron loss), and have better heat dissipation, coil windings, and sensor installation spaces. Still, the magnetic poles of the 3-pole magnetic bearings are asymmetric. The strong nonlinearity caused by magnetic flux coupling increases the difficulty of designing control systems [25]. It has three driving modes: First, two power amplifiers are used for driving, and the three magnetic poles of the magnetic bearing must be placed in a Y-shape. This method has no controllable bearing capacity in the opposite direction of gravity. It can only use the offset magnetic flux to generate a suspension force to overcome the gravity of the rotor. Its structural topology is shown in Figure 4a; second, three DC power amplifiers drive the 3-pole magnetic bearing to produce a radial two-degree-of-freedom suspension force (refer to Figure 4b). However, the currents of the three magnetic poles are independent of each other, and the spatial asymmetry of the three poles leads to coupling between the two degrees of freedom in the radial direction, which has little impact on the controller. The disadvantages of this type of driving mode are significant power losses and high costs; finally, a three-phase inverter is used to drive the 3-pole magnetic bearing. This driving mode has the advantages of small volumes, low costs, and low power losses. Therefore, it is more suitable for the 3-pole magnetic bearings. The three-phase inverter topology for a three-phase power amplifier is shown in Figure 4c [26,27].

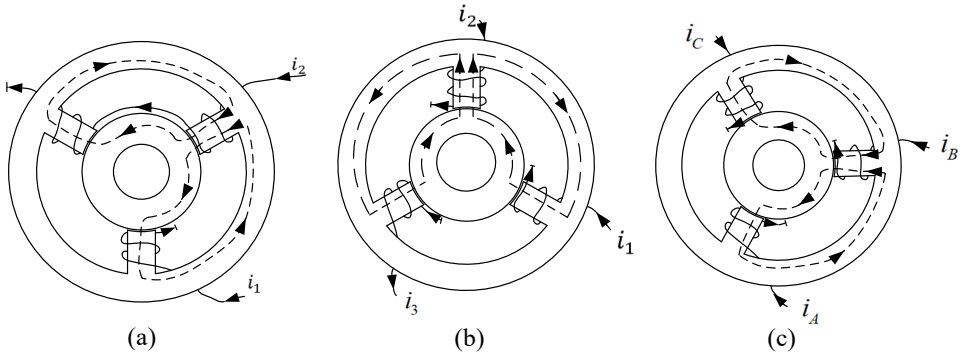

Figure 4. The 3-pole RMB structure. (**a**) Two power amplifier drive models. (**b**) Three-power amplifier drive models. (**c**) Three-phase drive models.

Two power amplifiers are used in Figure 4a. The two magnetic poles above the two power amplifiers can share a bias current and a control current, so the two DC power amplifiers can drive a 3-pole magnetic bearing. The upper two magnetic poles control

the displacement in the X-direction, and the lower pole controls the displacement in the Y-direction. In Figure 4c, the three-phase power inverter drives and changes the bias flux. The electromagnetic force generated by the three magnetic poles will change because the control current is switched between positive and negative. The three-phase coordinates are transformed into two-phase coordinates by a 2/3 transformation, corresponding to the displacement and current in the X- and Y-directions, and the current of the magnetic bearing can be easily controlled by using pulse width modulation technology [28].

The mode of driving 3-pole RMBs by three power amplifiers will lead to large coupling between magnetic poles and high cost. To improve the bearing capacity and controllability of 3-pole RMBs, the researchers changed their three radial magnetic poles into six radial magnetic poles evenly distributed along the circumference. Usually, adding three active magnetic poles or three permanent magnet magnetic poles to achieve a more stable control effect eliminates the influence of asymmetric structure and finally forms a 6-pole RMB. There are mainly three structural forms: the first is to add three permanent magnet poles to form a 6-pole hybrid radial magnetic bearing (refer to Figure 5a) [29]; the second is to add three active magnetic poles to form a 6-pole active radial magnetic bearing, and the structural form is shown in Figure 5b [30]; the third type is a three-phase six-pole RMB, which a three-phase inverter can drive. The structural form is that the opposite two poles have the same coil winding method and are connected in series into one phase. Hence, the direction of control magnetic flux generated by each phase is the same, and the structural topology is shown in Figure 5c.

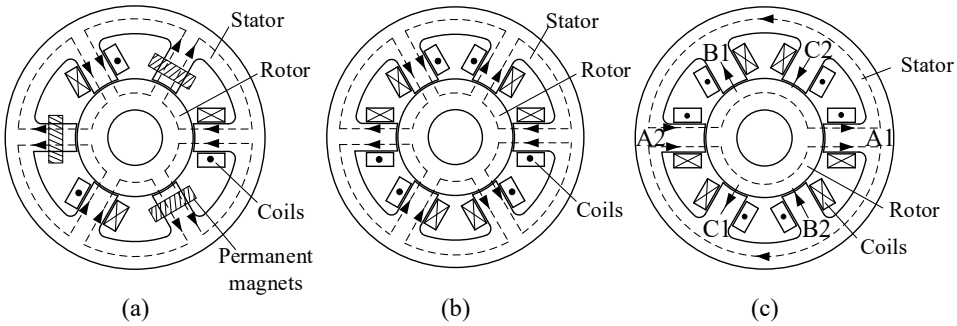

Figure 5. The 6-pole RMB structure. (**a**) Hybrid permanent magnet structure. (**b**) Six-power amplifier drive models. (**c**) Three-phase six-pole drive models.

The working model for a three-phase 6-pole RMB is that if the rotor deviates in the A2 direction, a positive control current must be applied to coils A1 and A2 to return the rotor to a balanced position. The control flux and bias flux generated by coil A1 are superimposed. The control and bias flux generated by coil A2 are offset, resulting in a proper force to return the rotor to its balanced position. Similarly, deviations in other directions can also be eliminated. The magnetic circuit is the most significant difference between 3-pole and 6-pole magnetic bearings. The 3-pole magnetic circuit is a C-type circuit formed by one of the magnetic poles and the other two magnetic poles, as shown in Figure 4a, while the 6-pole magnetic bearing is a C-type magnetic circuit formed by two magnetic poles, as shown in Figure 5b. The 6-pole RMB structure is better than the 3-pole RMB in carrying capacity and controllability, and the three-phase six-pole structure driven by the inverter is its unique advantage.

2.3. Eight-Pole RMBs and Twelve-Pole RMBs

The 4-pole RMBs are rarely used in harsh working environments, and their bearing capacity and fault tolerance limit their application range. The researchers optimized 4-pole RMBs and proposed the 8-pole magnetic bearing most widely used in industry and laboratory. The most frequently used are heteropolar 8-pole RMBs, which can be divided into two types according to the arrangement of radial magnetic poles. One type of magnetic pole is arranged as NNSS, and the structure is shown in Figure 6a. The structure can form

two types of structures according to the angle between the gravity direction (Y direction) and the nearest magnetic pole (0° or 22.5°). Its control methods are also different. The other is that the magnetic pole arrangement is NSNS (refer to Figure 6b), which has more significant advantages in redundant control. The strong coupling between magnetic poles allows redundant control [31,32].

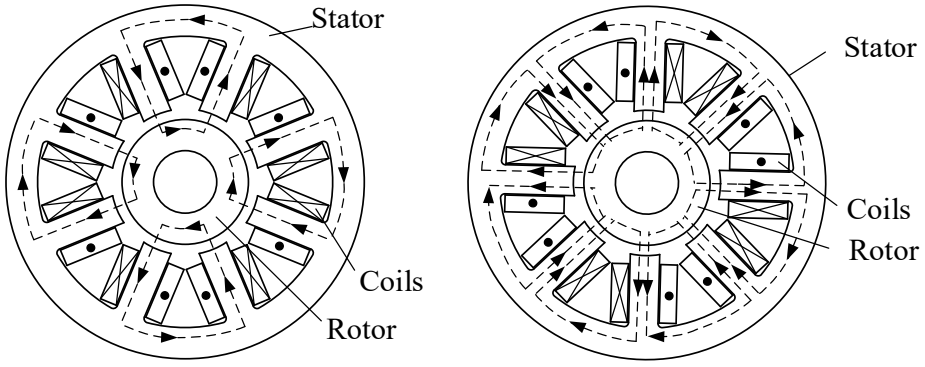

Figure 6. The 8-pole RMB structure. (**a**) NNSS structure of magnetic pole distribution. (**b**) NSNS structure of magnetic pole distribution.

In Figure 6a, the angle between the electromagnetic force of the 8-pole RMBs and the rotor gravity in the Y direction is 0°, and the angle between the electromagnetic force and the gravity can be formed by adjusting the magnetic pole is 22.5°. The control modes of the two magnetic pole structures are similar. Still, the included angle of the electromagnetic force is more favorable for the system to control the stable rotation of the rotor. Moreover, the magnetic flux coupling between the X and Y axes is lower, and the stability and accuracy of the follow-up control system are better. However, its magnetic pole's magnetic flux quickly falls into magnetic saturation when working under a heavy load [33,34]. The structure in Figure 6b has stronger mutual magnetic field coupling between magnetic poles, more serious control difficulty for the system than in Figure 6a, and higher power consumption. However, in the research on redundancy control, if one of the magnetic poles suddenly fails during the operation of the magnetic bearing, the redundancy control strategy designed in advance can prevent the magnetic bearing rotor from colliding, which is the unique advantage of the structure shown in Figure 6b.

In Figure 6a, its magnetic circuit is a typical C-type structure, and the magnetic pole slot is designed with an equal area. In practical applications, when the outer diameter of the stator of an RMB is large and the number of magnetic poles is small, standard C-type RMBs have problems, such as a large gap between the stator magnetic pole, which results in a waste of space in the magnetic bearing. The width of the stator magnetic pole cannot reach the maximum width, so the electromagnetic force generated by the radial electromagnetic bearing is not the maximum force [35].

The so-called E-type magnetic bearing is that one magnetic pole of the C-type structure is divided into two small magnetic poles and placed on both sides of the other magnetic pole. The two magnetic poles with a small area are called sub-magnetic poles, and the magnetic pole with a large middle area is called a central magnetic pole [36]. In general, the area of the auxiliary magnetic pole is half of the area of the central magnetic pole, and the number of turns of the coil is also half of the number of turns of the central magnetic pole. Therefore, as shown in Figure 7, the 12-pole E-type magnetic bearing structure is optimized by the 8-pole C-type structure [37].

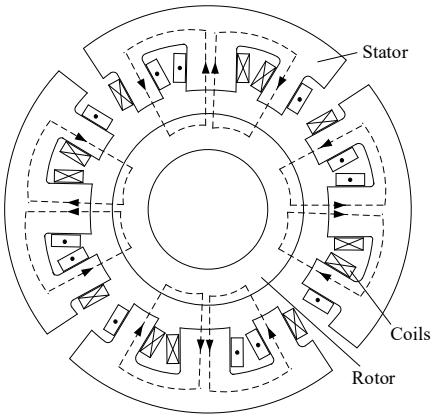

Figure 7. The 12-pole RMB E-type structure.

The original relatively large magnetic pole spacing and gap have been fully utilized due to the increased number of magnetic poles and windings. The E-type magnetic pole structure is usually distributed as SNS or NSN. Each magnetic pole group ensures the independence of the magnetic circuit and can suppress the influence between the magnetic circuits of adjacent magnetic pole groups. The magnetic pole distribution in Figure 7 is NSN. The performance of 12-pole RMBs is superior in terms of bearing capacity and controllability, and the magnetic field coupling between magnetic poles is low, which is widely used in the particular working environment.

2.4. Equivalent Magnetic Circuit Analysis

Equivalent magnetic circuit theory is a relatively intuitive and straightforward magnetic field calculation method that can easily and quickly determine the relevant structural parameters of a magnetic field. The magnetic circuit method is widely used for designing the structures of RMBs, and it accounts for the influences of magnetic leakage, the stator core, and rotor reluctance. However, the nonlinear material characteristics are ignored in these calculations. The magnetic circuit method is used for designing the structures of RMBs, accounting for the influences of magnetic leakage, the stator core, and rotor reluctance. The nonlinear material characteristics are ignored in these calculations, and the theoretical analyses and calculations are performed using the Maxwell equation. For engineering applications, the design of the magnetic field is achieved by using the equivalent magnetic circuit to convert the calculation of the magnetic field into the magnetic circuit, thereby converting the distributed parameter problem into the calculation of the concentrated parameter, which can simplify the calculation and ensure a sure accuracy [38]. Under the condition of neglecting the leakage of the magnetic pole and equal magnetic induction intensity of the air gap, this paper takes the commonly used 8-pole RMBs as an example to analyze its equivalent magnetic circuit.

There are some similarities between the magnetic circuit and the circuit, but the magnetic leakage phenomenon in the magnetic circuit is more severe than that in the circuit. The calculation in the magnetic circuit follows Ohm's law, and the direction of the magnetomotive force is the same as the positive direction of the power supply [39,40]. Figure 8a shows an 8-pole RMB with a magnetic pole distribution of NNSS, and Figure 8b shows an 8-pole RMB with a magnetic pole distribution of NSNS. The magnetic circuit and magnetic pole strength of both are different. Figure 8c shows the E-type 12-pole RMB equivalent magnetic circuit. An auxiliary magnetic circuit is added to the C-type magnetic circuit, and three magnetic poles form a unique circuit with better control but more extensive power consumption.

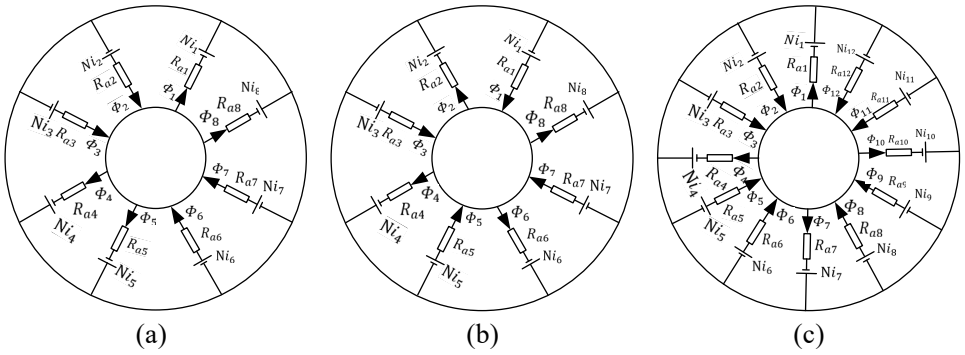

Figure 8. The 8-pole RMB equivalent magnetic circuits. (**a**) The magnetic circuit of NNSS magnetic pole distribution. (**b**) The magnetic circuit of NSNS magnetic pole distribution. (**c**) The magnetic circuit of 12 pole E-type structure distribution.

The equivalent magnetic circuit method is the most commonly used method to establish the electromagnetic force calculation model of magnetic bearing [41,42]. The equivalent magnetic circuit in Figure 8 includes the magnetomotive force (N_i), the magnetoresistance (R_a), and the magnetic flux (Φ). In a uniform magnetic circuit, according to Ohm's law of the magnetic circuit, the relationship among the three is:

$$N_i = R_a \Phi \tag{1}$$

The actual magnetic circuit is uneven and can be generally divided into several sections for calculation. The equivalent magnetic circuit can be obtained according to Kirchhoff's law, and the levitation force of the magnetic bearing can be deduced.

3. Structural Design and Simulation

The mechanical structure of the magnetic bearing is preliminarily designed as per the load requirements. Then, the actuator and power amplifier must be designed to build a complete magnetic bearing system. This paper gives the best structural design scheme with known bearing capacity and maximum outer diameter size. It analyzes its magnetic field saturation and the linear relationship between electromagnetic force and air gap through finite element analysis.

3.1. The 8-Pole RMBs Structure Design Process

The structural design of the magnetic bearing is different according to the application scenarios and functional requirements. The main calculation is the geometric structure parameters of the silicon steel sheet, the number of laminations, the number of coil turns, and the matching diameter of the stator rotor. At the same time, limiting conditions such as coil current and electromagnetic force are considered. Finally, the feasibility and reliability of the structure are analyzed through simulation [43,44]. In the paper, the parameters of the radial support are designed for the 8-pole RMBs in the high-speed rotating parts. The final structure must have minor wear, strong stability, and bearing capacity to meet the safety design requirements.

The specific design requirements are described next. The bearing capacity of the magnetic bearing is required to be 180 N, and the working efficiency of the magnetic bearing is the largest in the limited space. The maximum outer diameter of the stator is set to be 90 mm, the outer ring of the rotor and the stator are made of silicon steel sheets with a thickness of 0.3 mm, and the saturated magnetic field stress of the stator and rotor is selected to be 1.2 Tesla. According to the above design requirements, the parameters of the 8-pole RMBs are designed, and Figure 9 shows its structural geometry.

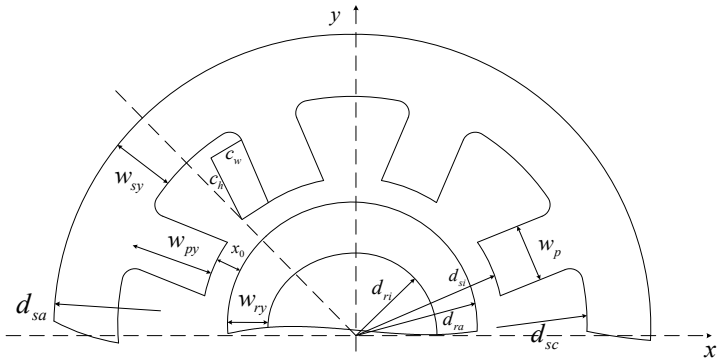

Figure 9. The 8-pole RMB geometry.

1. Air gap and related parameters;

The air gap length refers to the distance between the stator and the rotor. If the air gap is too large, the bearing capacity standard will become low, and if the air gap is too small, the control system will have high requirements. In engineering, when the rotor diameter is less than 100 mm, the air gap length (x_0) is generally between 0.3 and 0.6 mm, and this design is 0.5 mm. Generally, protective bearings are used to limit the rotor's runout range to prevent the magnetic bearing's sudden failure and the collision between the rotor and the stator. The air gap between the rotor and protective bearing is half that between the rotor and stator, indicating that the controllable range of actual runout is 0.25 mm.

Other relevant parameters are preliminarily set according to the known bearing capacity and air gap parameter information, which follow the conventional design experience. For example, the maximum bearing capacity (F_{max}) is 180 N. The parameters initially set are as follows: the rotor inner diameter (d_{ri}) is 15 mm, the stator yoke to pole width coefficient (c_{sy}) is 1, the pole length to pole width coefficient (c_{py}) is 2, the rotor yoke to pole width coefficient (c_{ry}) is 1.2, the silicon steel lamination coefficient (k_d) is 0.95, and the magnetic pole slot total rate (C_{coil}) is 0.7. These parameters can be adjusted according to the checking calculation and magnetic field analysis, and the final optimized coefficient can meet the design requirements.

2. Magnetic pole area and width;

According to Maxwell's attractive force formula, the total attractive force between the stator and rotor is:

$$F = B_0^2 A_0 / \mu_0 \tag{2}$$

B_0 is the magnetic induction strength in the air gap, and μ_0 is the air permeability. A_0 is the cross-sectional area of the air gap between the stator and the rotor. Given the maximum bearing capacity (F_{max}) and the saturated magnetic field strength (B_m), the formula for calculating the magnetic pole area can be obtained according to the derivation:

$$A_g = \frac{\mu_0}{k_d \cos \alpha} \cdot \frac{F_{\max}}{B_m^2} \tag{3}$$

where A_g is the magnetic pole area and α is the angle between the direction of electromagnetic force and the opposite direction of rotor gravity (Y direction). To keep the air gap uniform, the surface of the radial magnetic pole is not a plane but an arc surface, so the width (w_p) of the radial magnetic pole can be calculated according to the geometric relationship and relevant parameters. Factors such as coil installation, heat dissipation, and sensor installation space must be considered in actual processing. Therefore, a certain space margin must be reserved in the design.

3. Stator pole parameters and rotor dimensions;

According to the basic principle of magnetic circuit flow, saturation will not occur in the magnetic circuit if the average magnetic flux flowing through the stator yoke section is

greater than or equal to the average magnetic flux flowing through the radial magnetic pole root. Since the difference between the inner and outer diameters of the radial stator yoke shall not be less than half of the magnetic pole width(w_p), c_{sy} is selected as 1, and the width of the stator outer yoke (w_{sy}) is equal to the magnetic pole width. The magnetic pole length (w_{py}) and the rotor yoke width (w_{ry}) can be obtained according to the selected correlation coefficient.

The relevant size parameters of the magnetic pole are determined, and the total size of the stator's silicon steel sheet and the stator's inner and outer diameter can be obtained according to the geometric relationship. From the geometric structure diagram in Figure 9, the inner diameter (d_{sc})of the stator yoke, the inner diameter (d_{si}) of the stator, and the outer diameter (d_{ra}) of the rotor can be obtained, and the thickness (b) of the silicon steel sheet stack can be calculated according to the magnetic pole area.

4. Coil parameters;

The electromagnetic force is mainly generated by the electromagnet wound by the energizing coil, and the ampere-turns (NI) are the priority design parameter. A single coil's magnetic pole turns (N_p) can be calculated from the magnetic field strength and the maximum current (I_m). The approximate coil width (c_w) and coil length (c_h) can be obtained through the geometric structure, and then the inductance (L) and bus voltage (u_{dd}) of the coil can be calculated. Finally, in the case of ignoring magnetic leakage, one can simplify the magnetic bearing model and obtain the functional relationship between the electromagnetic force and the air gap and coil current. After Taylor series expansion, the electromagnetic force-displacement coefficient (k_x) and electromagnetic force current coefficient (k_i) can be obtained.

5. Design process and 3D model;

The actual bearing capacity of the magnetic bearing can be determined according to the stator and rotor dimensions and coil parameters. The design parameters are modeled in three dimensions, and ANSYS electronics analyze the magnetic field of the magnetic bearing to verify whether the electromagnetic force meets the requirements. Suppose the magnetic field distribution of the magnetic pole and the stator yoke shows saturation overload. In that case, the relevant setting coefficient can be adjusted, and the optimal design parameters can be obtained through continuous iterative optimization. Figure 10 shows the summarized mechanical structure design process of the 8-pole RMB.

The radial bearing capacity of the magnetic bearing is set as 180 N. Table 1 shows the structural parameters of a group of RMBs obtained according to the calculation in Figure 10.

Table 1. Structural parameters of the 8-pole RMB.

Parameter	Value
The outer diameter of the stator yoke (mm)	90
The inner diameter of the stator yoke (mm)	68
Stator thickness (mm)	30
Pole width (mm)	9
Air gap (mm)	0.5
Magnetic pole area (mm^2)	286
The outer diameter of the rotor (mm)	30
The inner diameter of the rotor (mm)	15
Turn ratio (At)	240

Figure 11 shows the 3D model established according to the design parameters, including silicon steel sheets (soft magnetic material), coils, mounting block, bearing seat, end cover, protective bearing, limit screw, and pressure ring. The installation block assembly fixes the silicon steel lamination. The limit screw is used to fix the protective bearing, and

the end cap and bearing shaft are used to install the magnetic bearing device on the fixed equipment.

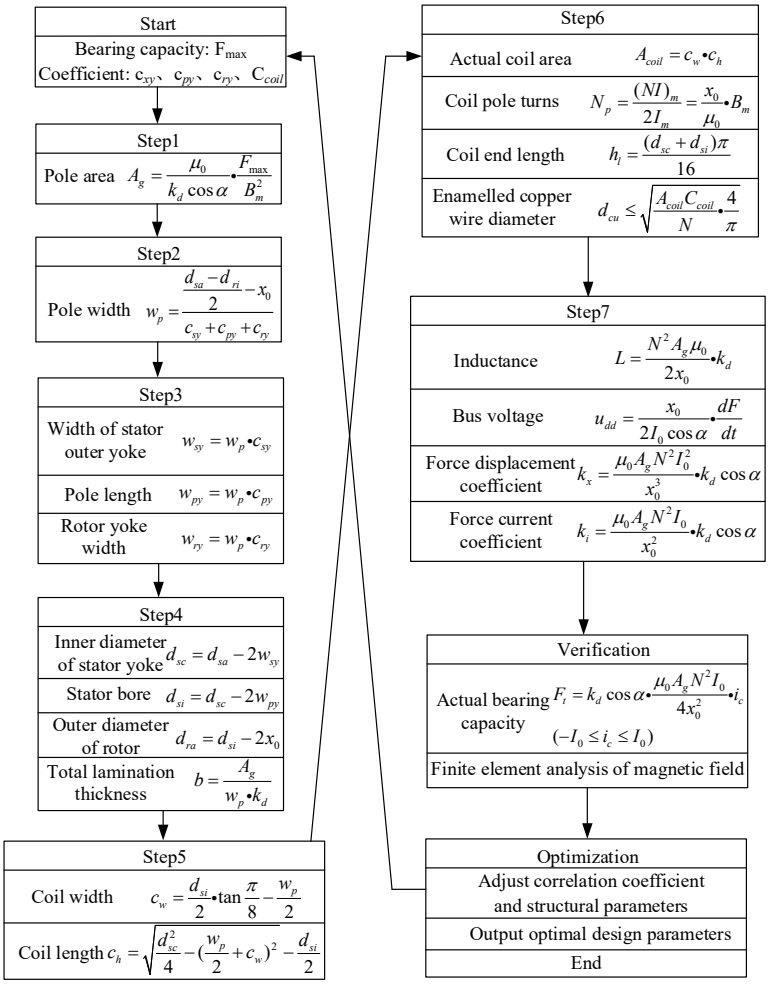

Figure 10. The 8-pole RMB design process.

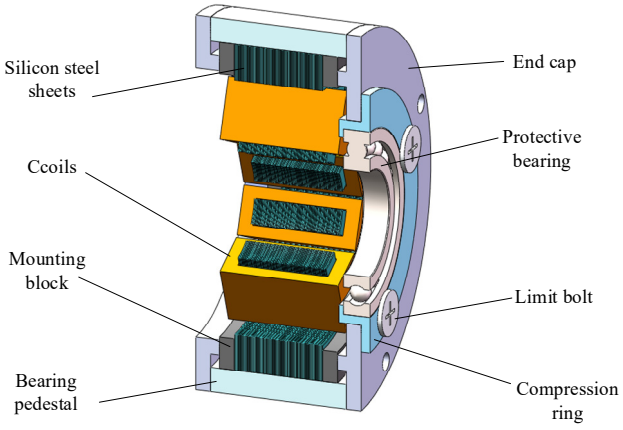

Figure 11. The 8-pole RMB 3D model.

The design method of magnetic bearing proposed in this paper is based on the maximum outer diameter of the stator with known geometric parameters of the stator. However, there are other design methods for different application requirements. If the rotor outer diameter parameter has been set, the magnetic pole area and coil ampere turns can be derived. Then, one can set the coefficient and get the geometric parameters of the stator

through the geometric relationship. Finally, the optimal design parameters can be obtained after correction, adjustment, and magnetic field analysis.

3.2. Magnetic Field Analysis and Verification

A magnetic bearing is a device that converts electromagnetic energy into mechanical energy. When the main shaft is suspended, there is a strong electromagnetic field in the magnetic bearing's radial or axial internal space. The distribution and variation of the electromagnetic field in different media determine the running state and performance of the magnetic suspension spindle. The stator rotor structural parameters of the magnetic bearing are preliminarily determined, and the feasibility of the structure needs to be verified in combination with the magnetic field analysis. Whether the magnetic field distribution and electromagnetic force meet requirements must be verified. The analysis is carried out for the proposed heteropolar RMB structure. The magnetic field cloud diagram shown in Figure 12 includes the 8-pole RMB of type C and the 12-pole RMB of type E.

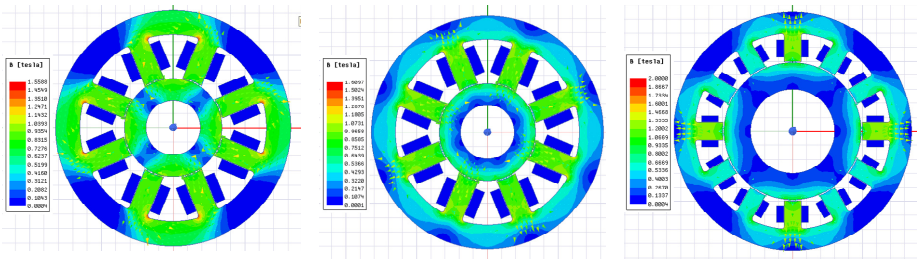

Figure 12. Magnetic field analysis of 8-pole and 12-pole RMBs. (**a**) Finite element analysis of 8-pole C-type structure. (**b**) Finite element analysis of 8-pole NSNS pole structure. (**c**) Finite element analysis of 12 pole E-type structure.

The two 8-pole magnetic bearings set the same ampere turns, but the winding methods of coils are different, resulting in two simulation results (a) and (b) in Figure 12. In practice, the effectiveness of the simulation can be verified by measuring the magnetic field strength around the coil with a Gauss meter. Figure 12a shows the magnetic field analysis of Figure 8a, which shows that the magnetic field coupling between the magnetic poles is weak. Still, the magnetic field strength is saturated at the chamfer of the magnetic pole column. When there is a margin in the magnetic pole space, the width can be increased to mitigate the influence of magnetic saturation, and the sharp angle radian can be smoothed. Figure 12b shows the magnetic field analysis for the Figure 8b structure. The analysis results show that one pole column needs to bear the magnetic field strength of two adjacent poles. Its air gap magnetic density is evenly distributed and formed by the superposition of adjacent magnetic circuits. The magnetic field strength of the magnetic pole column in Figure 12b is lower than that in Figure 12a. Still, the magnetic field coupling between the magnetic poles is large, and the system control difficulty is increased. The magnetic field analysis in Figure 12c shows that the magnetic circuit in Figure 8c can reduce the coupling between magnetic poles. Each group of magnetic poles is composed of three magnetic poles, and the magnetic field distribution is relatively uniform. Since the electromagnetic force of the E-type structure is mainly concentrated in the middle central magnetic pole, the controllability and bearing capacity of Figure 12c are greatly improved compared with the magnetic pole structure in Figure 12a, which is more favorable than the resultant force of the C-type structure. Therefore, the E-type structure is more widely used in the case of large structure volumes.

The material characteristics of silicon steel sheets determine the magnetic bearing's upper limit of magnetic field intensity. The linear control of the system requires that the magnetic field intensity changes in a linear range. Then, the reference point is selected in the magnetic circuit direction of the 8-pole magnetic bearing structure to reflect the

magnetic field intensity change characteristics. As shown in Figure 13, the magnetic field change and electromagnetic force of the designed 8-pole RMB are analyzed in the rotor outer yoke (m1), the stator pole post (m2), and the stator outer yoke (m3).

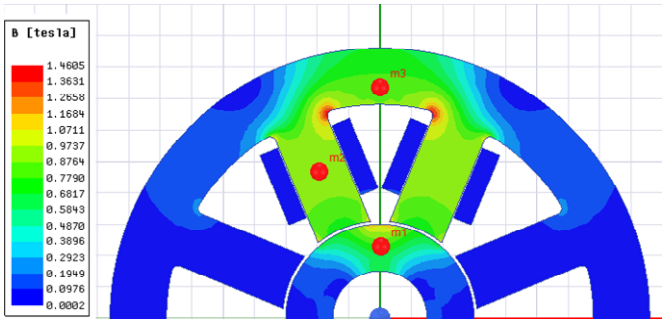

Figure 13. Magnetic field analysis of 8-pole RMBs magnetic pole.

The magnetization characteristic curve (B-H) and hysteresis loop of silicon steel sheet material limit the variation range of magnetic induction intensity in the magnetic bearing. The following control system design needs to be considered when designing the body structure of the magnetic levitation bearing. The linearization control is relatively stable and easy to realize. An approximate linear interval in the B-H curve of soft magnetic material is an ideal magnetic induction strength control range, which affects the robustness and accuracy of the control system for magnetic bearing. The magnetic bearing system takes the position change of the rotor as the signal input and the electromagnetic force generated by the electromagnet as the output. The air gap width between the stator and the rotor is an essential factor affecting the control performance. The single side (Y direction) of the air gap in the 8-pole RMB proposed in this paper is 0.5 mm, and the protective bearing is half the air gap. The rotor is at the geometric center when the air gap is set to 0.5 mm. Figure 14a shows the change of magnetic induction intensity at m1, m2, and m3 when the coil current is 3A and the change of electromagnetic force between air gaps when the air gap changes. Figure 14b shows changes in magnetic induction intensity at m1, m2, and m3 when the current changes when the air gap is 0.35 mm, and changes in electromagnetic force between the air gaps when the current changes.

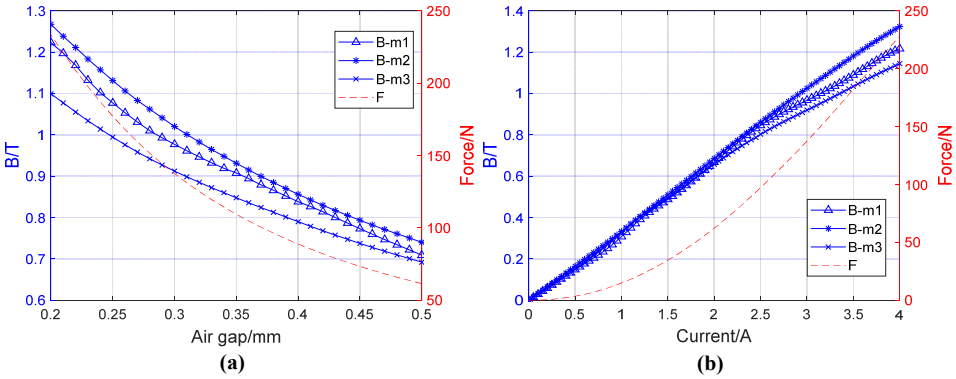

Figure 14. Change the trend of magnetic field intensity at three reference points (**a**) Air gap variation and magnetic field analysis. (**b**) Current variation and magnetic field analysis.

From Figure 14a, the magnetic induction intensity at m2 (magnetic pole column) is the largest, approximately linear, when the air gap changes from 0.35 to 0.5 mm, and does not exceed the saturation intensity of magnetic induction by 1.2 Tesla. The results show that the system can achieve good control performance within the runout range of 0–0.25 mm, and the electromagnetic force meets the design standard. Figure 14b shows that the electromagnetic force changes linearly within the current range of 2.5A−4A, and

the magnetic induction intensity at m2 changes approximately linearly with the current increase, indicating that the rotor can achieve approximately linear control within the safe range. There is usually interference between the two magnetic circuits, which leads to loss. To explore the loss between the magnetic circuits of the designed structure, 8-pole magnetic bearings arranged in NNSS are selected as the object. As shown in Figure 15, two close magnetic pole reference points, m1 and m2, are selected from the two C-type circuits, the reference point m3 of the outer magnet yoke of the rotor of the intermediate structure and the reference point m4 of the outer magnet yoke of the stator. In addition, m5 represents the reference point of the outer magnet yoke in the C-type circuit.

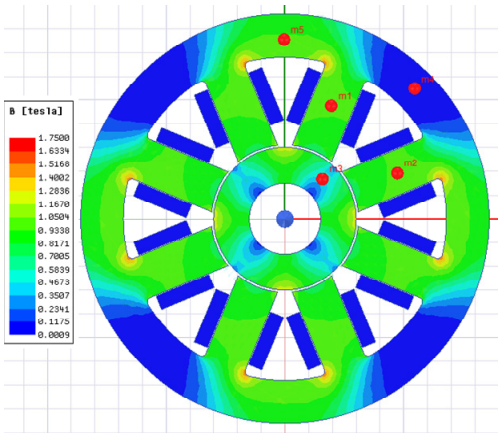

Figure 15. C-type magnetic circuit magnetic field simulation of 8-pole RMBs.

Compared with Figure 13, only the independent C-type magnetic circuit is simulated. Figure 15 contains the mutual loss between magnetic circuits. The magnetic field intensity of the magnetic pole is lower in Figure 15 with the same ampere-turns. According to the magnetic field changes at five reference points, the losses of two C-type magnetic circuits are studied, and the results are shown in Figure 16.

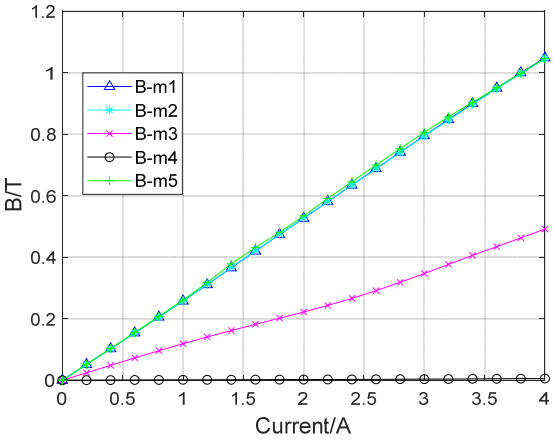

Figure 16. Change magnetic field intensity at the reference point of two C-type magnetic circuits.

Figure 16 shows that the magnetic field intensity changes at the reference point m1 and m2 of the C-type magnetic circuit are consistent because the currents in the two magnetic circuits are the same. In practice, to counteract the rotor gravity, the magnetic field intensity at m1 is higher than at m2. The magnetic field strength of reference point m5 is approximately m1, which indicates that the structural parameters of the magnetic pole and the outer yoke are suitable, and magnetic saturation is not easy to occur in the magnetic circuit. The magnetic field strength of reference points m3 and m4 is relatively high, and the magnetic field strength of m4 is 0, indicating that the interference between the two

C-type magnetic circuits is minor, which is conducive to reducing manufacturing costs. The above results of magnetic field analysis can show that the designed 8-pole RMBs structure meets the design requirements and the following system control design requirements.

4. Structural Optimization

The previous section gives the preliminary design of the structure in 8-pole RMBs. Still, the design will differ from the expected goal under different working environments and load-bearing requirements in practical applications. This section aims at optimizing the structure to improve the bearing capacity when the magnetic field strength in the magnetic circuit does not reach the material limit and provides a reference for the magnetic bearings under similar working conditions.

From the design process in the previous chapter and the magnetic field analysis of the electromagnetic force, current, and air gap, under the condition of limiting the current and the number of coils, magnetic pole width (w_p) impacts the electromagnetic force. At the same time, the coefficients of c_{sy}, c_{py}, and c_{ry} mainly determine the pole's width. According to the design flow chart, the three critical coefficients are optimized to improve the bearing capacity. Given the variation range of each coefficient, the variation trend of the coefficient and other parameters in Figure 15 can be obtained through the geometric relationship between structures.

The given variation range of c_{sy} is 0.7 to 1.2, the range of c_{py} is 1 to 2, and the variation range of c_{ry} is 0.5 to 1. The above variation range is determined by preventing magnetic field saturation during structure design and previous experience. Among the three coefficients, the variation range of c_{py} is the largest, which has the most significant impact on the optimization of the structure, so the optimization of this parameter is the main one. Figure 17a shows the influence of c_{py} on other parameters when a single coefficient changes, including the designed coil cavity area (A_c), the actual coil sectional area (A_{coil}), and the maximum magnetic pole area (A_m). It also shows the linear influence on the width of the magnetic pole. Figure 17b shows the influence of c_{py} on the area based on the magnetic pole width when the two coefficients c_{sy} and c_{py}, change simultaneously. Figure 17c–e show the changing trend of each coefficient when the three coefficients of c_{sy}, c_{py}, and c_{ry} change at the same time and the related influence.

The changing trend of a–e in Figure 17 shows the following results. With the increase of coefficient changes, the area of the maximum magnetic pole and the coil cavity increase slightly. In contrast, increasing the coefficient value can effectively reduce the gap between the designed area of the coil cavity and the area of the coil cross-section and can effectively improve the space utilization of the structure. The approximate range of the three coefficients can be further determined. The variation range of the coefficient c_{sy} should be greater than 0.85, the coefficient c_{py} should not be less than 1.3, and the coefficient c_{py} should be greater than 0.65. A more accurate variation range and influence coefficient trend are conducive to further optimization. Figure 17f shows the influence of the magnetic field force (F_t) when the three coefficients change. The value of the three coefficients can be obtained when reaching the design requirement of 180 N bearing capacity, but whether the value is optimal needs to be further verified.

The specific range of the three coefficients is known, so it is necessary to find the best coefficient value within this range. In this section, genetic algorithm optimization is taken as an example to obtain the best structure parameters through iterative optimization of coefficients. Through function fitting of the influence of coefficient in Figure 17f on bearing capacity, Equations (4)–(6) can be obtained, respectively, as the applicability function of the algorithm.

$$F_t = \frac{146.9}{c_{sy} - 0.15} \tag{4}$$

$$F_t = \frac{293.8}{c_{py} + 0.1} \tag{5}$$

$$F_t = \frac{146.9}{c_{ry} + 0.05} \tag{6}$$

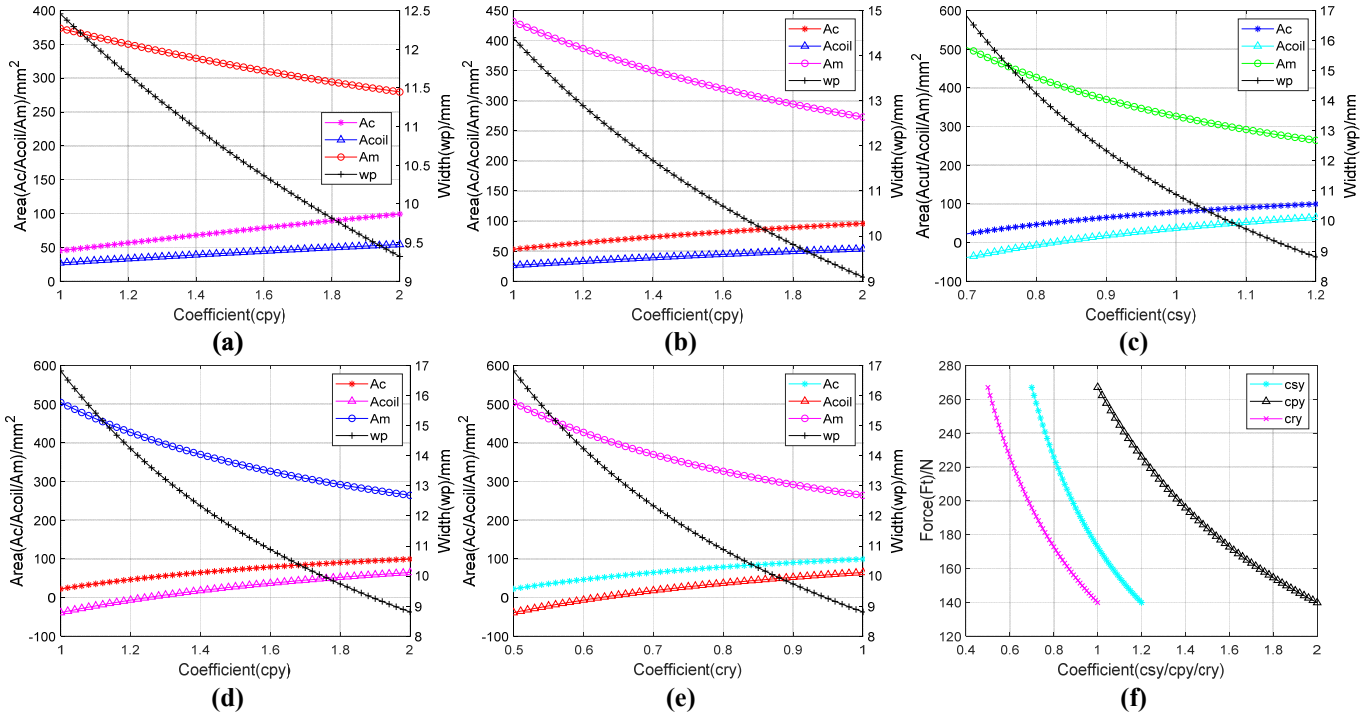

Figure 17. Influence of three coefficient changes on the structure. (**a**) Effect of independent change of coefficient c_{py}. (**b**) Influence of two coefficient changes of c_{py}. (**c**) Three coefficient variation c_{sy} trend. (**d**) Three coefficient variation c_{py} trend (**e**) Three coefficient variation c_{ry} trend. (**f**) Three coefficient variation F_t trend.

According to the changing trend of A_c and A_{coil} in Figure 15, there is a gap between them when limiting the coefficient change range, indicating that magnetic saturation will not occur when increasing the width of the magnetic pole. The optimization is carried out to change the maximum influence coefficient c_{py}. Equation (7) is the function of the influence on the A_m of the magnetic pole area when the c_{py} changes. The geometric relationship will be (4)–(7) to form the genetic algorithm's fitness function, with the maximum bearing capacity as the output and the iterative optimization of the coefficient.

$$A(x) = 276.6(\sin(x - \pi)) + 12.45((x - 10)^2) - 277.2 \tag{7}$$

Three coefficients are optimized by genetic algorithm, and one group of optimization results is shown in the following. The maximum electromagnetic force finally obtained is 249.25 N. The coefficients of c_{sy}, c_{py}, and c_{ry} obtained after data processing are 1.1, 1.76, and 0.87, respectively. The width of the magnetic pole deduced is 10 mm. Compared with the initially designed structure, the bearing capacity is improved, and no magnetic saturation occurs, which shows that the optimization results of the algorithm are effective.

In this section, the genetic algorithm optimization is employed to verify the feasibility of the structural optimization scheme, mainly to optimize the magnetic pole width and influence coefficient to improve the bearing capacity. Other aspects of optimizing the structure include increasing the number of ampere-turns of the coil and increasing the width of the magnetic pole to prevent magnetic saturation, which can effectively improve the bearing capacity.

5. Conclusions

This paper analyzed the parameter designs, equivalent magnetic circuits, and magnetic fields of different RMB structural topologies and summarized various design methods and advantages. The conclusions are as follows:

1. The 3-pole RMB is a strongly coupled nonlinear system, and its control is difficult. In contrast, an optimized 6-pole magnetic bearing has higher bearing capacity and stability.
2. A commonly used 8-pole magnetic bearing performs better than a 4-pole magnetic bearing. However, the magnetic pole produces magnetic saturation quickly, and optimizing the structural parameters can be used to reduce the impact.
3. The 12-pole E-type RMB is superior to the standard 8-pole C-type RMB in carrying capacity, stability, and control performance, but it has high energy consumption and few applications.

After induction, the most commonly used 8-pole RMB structure is selected as the primary design goal, and the structural design scheme is proposed. Then, the genetic algorithm is used to optimize the influence coefficient of the structure, and the obtained structure can effectively improve the bearing capacity. The optimization method provides a reference for the structure design of magnetic bearings in practical applications.

The challenging problems of magnetic bearings need to be studied and considered in future engineering applications and optimization design. There are several main aspects: first, classification and parameterization of magnetic bearing based on application scenarios, matching different magnetic bearing topologies, and finally, forming standardization of magnetic bearing design; second, the sensor, controller, and other components are integrated with the magnetic bearing device to form an integrated design; finally, according to the magnetic levitation control system, the integrated magnetic bearing is intellectualized to form self-perception, self-learning, self-diagnosis, and optimization.

Author Contributions: Methodology and review, H.W.; writing-original draft and editing, Q.L.; supervision, Y.H. All authors have read and agreed to the published version of the manuscript.

Funding: This research was funded by the National Key Research and Development Project of China, grant number 2018YFB2000103.

Institutional Review Board Statement: Not applicable.

Informed Consent Statement: Not applicable.

Data Availability Statement: Not applicable.

Acknowledgments: The project was supported by the National Key Research and Development Project of China with grant number 2018YFB2000103.

Conflicts of Interest: The authors declare no conflict of interest.

References

1. Srinivas, R.S.; Tiwari, R.; Kannababu, C. Application of active magnetic bearings in flexible rotordynamic systems—A state-of-the-art review. *Mech. Syst. Signal Process.* **2018**, *106*, 537–572. [CrossRef]
2. Ye, X.; Le, Q.; Zhou, Z. A Novel Homopolar Four Degrees of Freedom Hybrid Magnetic Bearing. *IEEE Trans. Magn.* **2020**, *56*, 1–4. [CrossRef]
3. Huang, T.; Min, Z.; Guangfeng, Z. A review of active magnetic bearing control technology. In Proceedings of the 2019 Chinese Control and Decision Conference (CCDC), Nanchang, China, 3–5 June 2019.
4. Wang, Z.; Zhang, T.; Wu, S. Suspension Force Analysis of Four-Pole Hybrid Magnetic Bearing with Large Radial Bearing Capacity. *IEEE Trans. Magn.* **2020**, *56*, 1–4. [CrossRef]
5. Tshizubu, C.; Santisteban, J.A. A simple PID controller for a magnetic bearing with four poles and interconnected magnetic flux. In Proceedings of the 2017 6th International Symposium on Advanced Control of Industrial Processes (AdCONIP), Taipei, Taiwan, 28–31 May 2017.
6. Liyan, G.; Zhongyuan, H.; Jiaqi, X.; Huimin, W.; Xinmin, L.; Shuang, W. Design and Analysis of Modulated Magnetic Pole for Dual Three-Phase Surface-Mounted Permanent Magnet Synchronous Motor. *Energies* **2022**, *15*, 4597.

7. Peng, B.; Tao, Z. Design and Analysis on the Novel Uncoupled Six-pole Three-Degree-of-Freedom Hybrid Magnetic Bearing. In Proceedings of the 2020 IEEE International Conference on Applied Superconductivity and Electromagnetic Devices (ASEMD), Tianjin, China, 16–18 October 2020.
8. Asama, J.; Oi, T.; Oiwa, T.; Chiba, A. Simple Driving Method for a 2-DOF Controlled Bearingless Motor Using One Three-Phase Inverter. *IEEE Trans. Ind. Appl.* **2018**, *54*, 4365–4376. [CrossRef]
9. Zhang, H.; Huangqiu, Z.; Mengyao, W. Multi-objective Parameter Optimization Based Design of Six-pole Radial Hybrid Magnetic Bearing. *IEEE J. Emerg. Sel. Top. Power Electron.* **2021**, *10*, 4526–4535. [CrossRef]
10. Liu, G.; Zhu, H.; Zhang, W. Principle and performance analysis for six-pole hybrid magnetic bearing with a secondary air gap. *Electron. Lett.* **2021**, *57*, 548–549. [CrossRef]
11. Ju, J.; Zhu, H. Radial Force-Current Characteristics Analysis of Three-Pole Radial-Axial Hybrid Magnetic Bearings and Their Structure Improvement. *Energies* **2016**, *9*, 706. [CrossRef]
12. Zhu, H.; Wang, S. Decoupling control based on linear/nonlinear active disturbance rejection switching for three-degree-of-freedom six-pole active magnetic bearing. *IET Electr. Power Appl.* **2020**, *14*, 1818–1827. [CrossRef]
13. Wu, C.; Hongkai, Z. Finite element analysis of eight-pole homopolar hybrid magnetic bearing. In Proceedings of the 2021 IEEE International Conference on Electrical Engineering and Mechatronics Technology (ICEEMT), Qingdao, China, 2–4 July 2021.
14. Wu, L.; Wang, D.; Su, Z.; Wang, K.; Zhang, X. Analytical Model of Radial Permanent Magnet Biased Magnetic Bearing with Assist Poles. *IEEE Trans. Appl. Supercond.* **2016**, *26*, 1–5. [CrossRef]
15. Sun, J.; Chen, D. Analysis and experiment of eddy current loss in Homopolar magnetic bearings with laminated rotor cores. *Acta Astronaut.* **2013**, *89*, 229–235.
16. Zhong, Z.; Duan, Y.; Cai, Z.; Qi, Y. Design and Cosimulation of Twelve-Pole Heteropolar Radial Hybrid Magnetic Bearing. *Math. Probl. Eng.* **2021**, *2021*, 8826780. [CrossRef]
17. Kumar, G.; Choudhury, M.D.; Natesan, S.; Kalita, K. Design and Analysis of a Radial Active Magnetic Bearing for Vibration Control. *Procedia Eng.* **2016**, *144*, 810–816. [CrossRef]
18. El-Shourbagy, S.M.; Saeed, N.A.; Kamel, M.; Raslan, K.R.; Aboudaif, M.K.; Awrejcewicz, J. Control Performance, Stability Conditions, and Bifurcation Analysis of the Twelve-Pole Active Magnetic Bearings System. *Appl. Sci.* **2021**, *11*, 10839. [CrossRef]
19. Zhang, W.; Zhu, H. Radial magnetic bearings: An overview. *Results Phys.* **2017**, *7*, 3756–3766. [CrossRef]
20. Zhang, W.; Wu, R.Q.; Siriguleng, B. Nonlinear Vibrations of a Rotor-Active Magnetic Bearing System with 16-Pole Legs and Two Degrees of Freedom. *Shock. Vib.* **2020**, *2020*, 5282904. [CrossRef]
21. Kandil, A. Investigation of the whirling motion and rub/impact occurrence in a 16-pole rotor active magnetic bearings system with constant stiffness. *Nonlinear Dyn.* **2020**, *102*, 2247–2265. [CrossRef]
22. Kandil, A.; Sayed, M.; Saeed, N.A. On the nonlinear dynamics of constant stiffness coefficients 16-pole rotor active magnetic bearings system. *Eur. J. Mech. A/Solids* **2020**, *84*, 104051. [CrossRef]
23. Sun, J.; Ju, Z.; Peng, C.; Le, Y.; Ren, H. A Novel 4-DOF Hybrid Magnetic Bearing for DGMSCMG. *IEEE Trans. Ind. Electron.* **2016**, *64*, 2196–2204. [CrossRef]
24. Fang, J.; Wang, X.; Wei, T.; Tang, E.Q.; Fan, Y.H. Homopolar 2-Pole Radial Permanent-Magnet Biased Magnetic Bearing with Low Rotating Loss. *IEEE Trans. Magn.* **2012**, *48*, 2293–2303.
25. Hemenway, N.R.; Severson, E.L. Three-Pole Magnetic Bearing Design and Actuation. *IEEE Trans. Ind. Appl.* **2020**, *56*, 6348–6359. [CrossRef]
26. Hemenway, N.R.; Severson, E.L. Exact Force Vector Regulation of the Three-Pole Magnetic Bearing. *IEEE Trans. Ind. Appl.* **2021**, *57*, 7024–7034. [CrossRef]
27. Debnath, S.; Biswas, P.K.; Laldingliana, J. Analysis and simulation of PWM based power amplifier for single axis Active Magnetic Bearing (AMB). In Proceedings of the 2017 IEEE Transportation Electrification Conference (ITEC-India), Pune, India, 13–15 December 2017.
28. Wajnert, D. Analysis of the cross-coupling effect and magnetic force nonlinearity in the 6-pole radial hybrid magnetic bearing. *Int. J. Appl. Electromagn. Mech.* **2019**, *61*, 43–57. [CrossRef]
29. Adascalitei, C.; Radu, M.; Claudia, M. General approach of radial active magnetic bearings design and optimization. In Proceedings of the 2021 International Conference on Electrical Drives & Power Electronics (EDPE), Dubrovnik, Croatia, 22–24 September 2021.
30. Zhihao, M.; Gai, L.; Yichen, L.; Zhaocheng, Y.; Huangqiu, Z. Research of a Six-Pole Active Magnetic Bearing System Based on a Fuzzy Active Controller. *Electronics* **2022**, *11*, 1723.
31. Cheng, X.; Deng, S.; Baixin, C.; Yefa, H.; Huachun, W.; Rougang, Z. Design and implementation of a fault-tolerant magnetic bearing control system combined with a novel fault-diagnosis of actuators. *IEEE Access* **2020**, *9*, 2454–2465. [CrossRef]
32. Cheng, X.; Deng, S.; Baixin, C.; Meiqian, L.; Rougang, Z. Optimization of bias current coefficient in the fault-tolerance of active magnetic bearings based on the redundant structure parameters. *Automatika* **2020**, *61*, 602–613. [CrossRef]
33. Kang, K.; Alan, P. Homopolar magnetic bearing saturation effects on rotating machinery vibration. *IEEE Trans. Magn.* **2012**, *48*, 1984–1994. [CrossRef]
34. Gerami, A.; Paul, A.; Roger, F. Control of magnetic bearing with material saturation nonlinearity. *J. Dyn. Syst. Meas. Control.* **2015**, *137*, 061002. [CrossRef]
35. Xu, S.; Fang, J. A novel conical active magnetic bearing with claw structure. *IEEE Trans. Magn.* **2013**, *50*, 1–8.

36. Wang, H.; Bingkun, X.; Shaofei, T. Modeling and analysis of E-Core permanent magnet biased radial magnetic bearing. *Int. J. Appl. Electromagn. Mech.* **2015**, *49*, 179–193. [CrossRef]
37. Saeed, N.A.; El-Shourbagy, S.M.; Kame, M.; Raslan, K.R.; Aboudaif, M.K. Nonlinear dynamics and static bifurcations control of the 12-pole magnetic bearings system utilizing the integral resonant control strategy. *J. Low Freq. Noise Vib. Act. Control.* **2022**, 1–29. [CrossRef]
38. Zhang, X.; Liu, X.; Han, B.C.; Ye, X.Y. Magnetic circuit designing and structural optimisation for a three degree-of-freedom hybrid magnetic bearing. *IET Electr. Power Appl.* **2018**, *12*, 1082–1089.
39. Zhu, R.Z.; Xu, W.; Ye, C.Y.; Zhou, J.G.; Lei, G.; Li, X. Design optimization of a novel heteropolar radial hybrid magnetic bearing using magnetic circuit model. *IEEE Trans. Magn.* **2017**, *54*, 1–5. [CrossRef]
40. Martynenko, G. Practical application of the analytical method of electromagnetic circuit analysis for determining magnetic forces in active magnetic bearings. In Proceedings of the 2020 IEEE Problems of Automated Electrodrive. Theory and Practice (PAEP), Kremenchuk, Ukraine, 21–25 September 2020.
41. Jiang, H.; Zhenzhong, S.; Dong, W. Analytical Calculation of Active Magnetic Bearing Based on Distributed Magnetic Circuit Method. *IEEE Trans. Energy Convers.* **2020**, *36*, 1841–1851. [CrossRef]
42. Chunmin, Y.; Zhiquan, D.; Shangsi, C.; Lei, M.; Cong, P.; Xin, C. A novel subdomain and magnetic circuit modeling method for hybrid homopolar radial magnetic bearings. *Mech. Syst. Signal Process.* **2022**, *170*, 108823.
43. Le, Y.; Kun, W. Design and optimization method of magnetic bearing for high-speed motor considering eddy current effects. *IEEE/ASME Trans. Mechatron.* **2016**, *21*, 2061–2072. [CrossRef]
44. Lv, H.; Geng, H.; Jian, Z.; Du, T.; Hao, L. Structure design and optimization of thrust magnetic bearing for the high-speed motor. In Proceedings of the 2017 IEEE International Conference on Mechatronics and Automation (ICMA), Takamatsu, Japan, 6–9 August 2017.